Journal of Materials Chemistry A

COMMUNICATION

View Article Online
View Journal | View Issue

Lithium storage in a highly conductive Cu_3Ge boosted Ge/graphene aerogel†

Chuanjian Zhang,[a] Fenglian Chai,[ab] Lin Fu,[a] Pu Hu,[a] Shuping Pang[a] and Guanglei Cui*[a]

Cite this: *J. Mater. Chem. A*, 2015, **3**, 22552

Received 31st August 2015
Accepted 5th October 2015

DOI: 10.1039/c5ta06862b

www.rsc.org/MaterialsA

A Cu_3Ge/Ge@G aerogel was employed as an anode for a lithium-ion battery by a simple pyrolysis of a $CuGeO_3$ nanowire and graphene oxide nanosheet mixture. It is demonstrated that both the Cu_3Ge nanoparticles and graphene nanosheets act as conductive buffers to accelerate the electron migration rate and enhance the cycling stability of the electrode.

Introduction

Germanium (Ge) is considered as one of the most promising candidates for next generation lithium-ion battery anodes due to its high specific capacity (1384 mA h g^{-1} according to $Li_{15}Ge_4$).[1–4] Compared with silicon (Si), a superior electronic conductivity and lithium diffusivity enable germanium to be more attractive for high power applications.[5,6] However, similar to Si and Sn which are also limited by a huge volume change during lithiation (over 300%), Ge suffers from severe capacity fade and limited applications.[7–9] With the aim of addressing this tough issue, considerable efforts have been dedicated to developing Ge-based anodes with long-term cycling performance. One of the two successful routes is to downsize the particles to nanoscale. For example, Ge nanostructures with one dimensional features such as nanowires,[10,11] nanotubes and nanorods[12] could relieve the stress generated from the lithiated volume variation and maintain good structural integrity. Benefiting from this nanosize effect, the cycling performances of Ge-based anodes could be enhanced. The other efficient strategy is to disperse active Ge particles into a buffer matrix.[13] Various carbonaceous materials have been commonly employed for their conductive and elastic merits.[2,7,14] Among these, graphene[15,16] and carbon nanotubes[17,18] are more attractive for their superb conductive features. Hence, considerable Ge/graphene and Ge/carbon nanotube composite anodes have been reported with improved cycling stability. Nowadays, ternary germinate oxides ($M_xGe_yO_z$, M = Cu, Zn, Pb, Fe, Ba, Sr, Ca)[19–23] which could be easily synthesized *via* simple hydrothermal reactions show promising applications in low cost anodes. Owing to the *in situ* formed Li_2O which acts as a buffer matrix, the volume expansion of Ge was alleviated and improved cycling performances were recorded.[24,25] However, just the lithium consumption required for Li_2O formation leads to a low initial coulombic efficiency (<70%) in these materials. It is reported that a decrease of oxygen content in anode materials is helpful to improve the initial coulombic efficiency. Recently, Kim's group synthesized a multiphase $Cu_3Ge/GeO_x/CuGeO_3$ nanowire anode which by partial reduction of the $CuGeO_3$ nanowires acquired an improvement in initial coulombic efficiency.[26] It is worth noting that Cu_3Ge possesses an extraordinarily high electrical conductivity of $(1–1.67) \times 10^7$ S cm^{-1}, which is much higher than that of pure Ge (1.45 S cm^{-1}). Hence, a Ge based anode with a conductive Cu_3Ge component may be expected to show favorable electrochemical performances. More recently, graphene based aerogels with a free-standing hierarchical nanostructure were employed as high performance anodes for lithium-ion batteries and supercapacitors.[27–29] However, the rational design and synthesis of novel Ge/graphene aerogels towards use in lithium-ion batteries is still a big challenge.

Herein, we presented a binder-free Cu_3Ge/Ge@G aerogel as the anode for a lithium-ion battery by a simple pyrolysis route under hydrogen atmosphere. When compared with a reported $CuGeO_3$ nanowire (NW) based anode, an improvement in the initial coulombic efficiency was achieved for the Cu_3Ge/Ge@G aerogel due to the absence of oxygen and the electrochemically inert additive. Meanwhile, graphene nanosheets act as a buffer for volume expansion of the Ge and result in a stable cycling performance. More importantly, a conductive network consisting of highly conductive Cu_3Ge and graphene enhanced the rate capability of the aerogel anode. These merits allow the Cu_3Ge/

[a]Qingdao Industrial Energy Storage Research Institute, Qingdao Institute of Bioenergy and Bioprocess Technology, Chinese Academy of Sciences, No. 189 Songling Road, Qingdao, 266101, PR China. E-mail: cuigl@qibebt.ac.cn

[b]College of Chemistry and Molecular Engineering, Qingdao University of Science and Technology, No. 53 Zhengzhou Road, Qingdao, 266042, PR China

† Electronic supplementary information (ESI) available. See DOI: 10.1039/c5ta06862b

Ge@G aerogel to be a promising anode material for high performance lithium batteries.

Experimental section

Synthesis of the Cu_3Ge/Ge@G aerogel

The graphene oxide nanosheet gel (GO) was synthesized by a modified Hummers method as reported elsewhere.[30] $CuGeO_3$ nanowires ($CuGeO_3$ NWs) were prepared *via* a hydrothermal method reported by the Yu group.[31] Next, a certain amount of $CuGeO_3$ NWs was mixed with the GO gel in 80 ml of deionized water, then treated by ultrasonication and stirred for 2 h. The well-dispersed suspension was transferred to a 100 ml stainless steel autoclave for hydrothermal reaction and incubated for 24 h. After cooling, the black $CuGeO_3$ NW/G hydrogel was freeze dried for another 24 h to obtain fluffy foams. For the synthesis of the Cu_3Ge/Ge@G aerogel, $CuGeO_3$/G foams were annealed at 550 °C for 1 h under H_2 atmosphere. The Cu_3Ge/Ge material was synthesized by direct pyrolysis of $CuGeO_3$ NWs.

Material characterization

X-ray diffraction (XRD) patterns of samples were recorded on a Bruker-AXS Micro-diffractometer (D8 ADVANCE) with Cu Kα radiation ($\lambda = 1.5406$ Å) from 10° to 80° at a scanning speed of 4° min^{-1}. Morphology details and lattice structural information were examined using field emission scanning electron microscopy (FESEM, HITACHI S-4800) and high-resolution transmission electron microscopy (HRTEM, TECNAI F20 ST). Raman spectroscopy data were acquired on a Bruker TENSOR 27 spectrometer inside an Ar-purged chamber. X-ray photoelectron spectroscopy (XPS) was performed using an ESCALab 220i-XL spectrometer (VG Scientific) with Al Kα radiation in twin anodes at 14 kV × 16 mA. TG-DTA (SDT Q600 V8.0 Build 95, Universal V4.0C TA Instruments, USA) was conducted under air atmosphere with a flow rate of 40 ml min^{-1} from room temperature to 800 °C at 10 °C min^{-1}.

Thermogravimetric analysis (TGA) was carried out to determine the carbon content with a TGA/differential scanning calorimetry (DSC) type instrument (METTLER TOLEDO, Switzerland) at a heating rate of 10 °C min^{-1} from room temperature to 800 °C in air.

Electrochemical analysis

Electrochemical measurements were performed using CR2032 coin-type cells assembled in an argon-filled glove box. For the battery test, the Cu_3Ge/Ge@G aerogel was cut and compressed into a circular pellet with a diameter of 10 mm and directly employed as a cathode. For the Cu_3Ge/Ge material, the working electrodes were prepared by mixing active materials, superP, and poly(acrylic) acid binder in a weight ratio of 80 : 10 : 10 and pasting this onto copper foil followed by drying in a vacuum oven at 120 °C for 8 h. Li metal foil and polypropylene membrane (celgard 2500) were used as anode and separator, respectively. A liquid electrolyte (ethylene carbonate, dimethyl carbonate and dimethyl carbonate, 1 : 1 : 1 by volume) with 1.0 M $LiPF_6$ and 2 wt% vinylene carbonate (VC) additive was applied as an electrolyte. Cyclic voltammetry (CV) was conducted by using an IM6 instrument at a scanning rate of 0.2 mV s^{-1} between 0.005 and 3 V. Electrochemical impedance spectroscopy (EIS) measurements were carried out using a ZAHNER ZENNIUM electrochemical workstation.

Results and discussion

A schematic illustration of the synthesis process of the Cu_3Ge/Ge@G aerogel is depicted in Fig. 1. $CuGeO_3$ NWs and GO nanosheets were prepared *via* a hydrothermal method and a modified Hummers method as reported, respectively. By mixing the two components followed by another hydrothermal treatment, the $CuGeO_3$ NW/G hydrogel was synthesized. At this stage, GO nanosheets were reduced to some extent. To prepare the Cu_3Ge/Ge@G aerogel, the $CuGeO_3$ NW/G aerogel was freeze dried and annealed at 550 °C for 1 h under H_2 atmosphere. Due to the reduction reaction, the $CuGeO_3$ NWs were decomposed to Cu_3Ge/Ge nanoparticles accompanying a complete removal of the oxygen-containing groups in the GO. SEM images of the $CuGeO_3$ NWs are shown in Fig. S1a.† It can be seen that the hydrothermally synthesized NWs are a few micrometers long with a diameter of 30 nm which is consistent with the reported result.[31] TEM images of the $CuGeO_3$ NW/G composite shown in Fig. S1b† indicate that the $CuGeO_3$ NWs are well enwrapped by the GO nanosheets. The XRD pattern of the nanohybrid is displayed in Fig. S2.† All the peaks can be indexed to the orthorhombic structured $CuGeO_3$ (JCPDS 32-0333) and no peaks of impurities were detected.

A typical XRD pattern of the Cu_3Ge/Ge@G aerogel is displayed in Fig. 2a. After being annealed under hydrogen atmosphere, the $CuGeO_3$ phase has been decomposed to Cu_3Ge and metallic Ge (JCPDS 04-0545)[26,32] without any impurities. It could be clearly seen from the SEM image in Fig. 2b that Cu_3Ge/Ge nanoparticles with a size of tens of nanometers were well-enwrapped by the graphene nanosheets. On one hand, the interconnected graphene in this unique structure could buffer the volume expansion of the lithiated Ge nanoparticles and improve the cycling performance of the electrode. On the other hand, the conductive network supported by graphene also boosts the electron migration of the electrode.[33–35] In addition, the inset in the SEM image confirmed that the Cu_3Ge/Ge@G aerogel kept a good cylindrical shape which could be easily cut as an anode for battery tests. A lot of wrinkles displayed in the TEM image (Fig. 2c) demonstrated that the graphene nanosheets were well-exfoliated. The graphene enwrapped Cu_3Ge/Ge

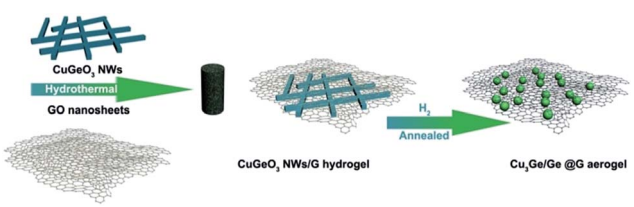

Fig. 1 Schematic illustration of the fabrication of the Cu_3Ge/Ge@G aerogel.

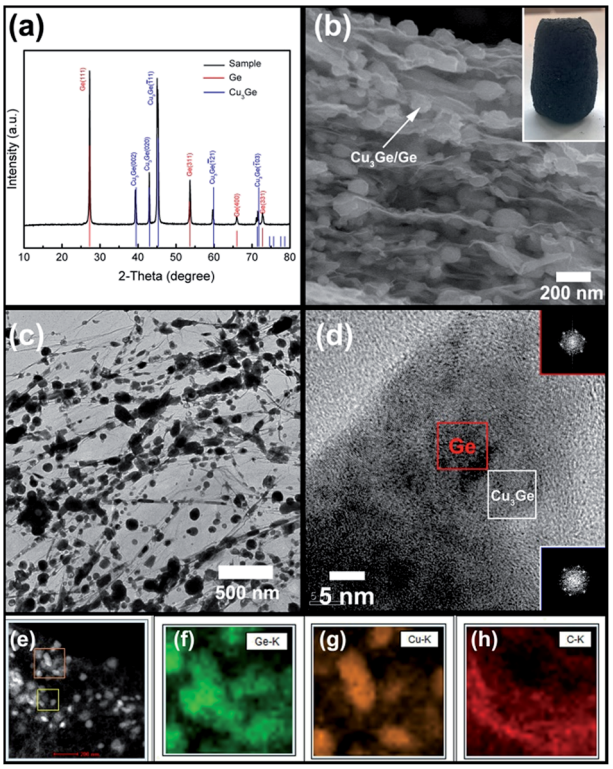

Fig. 2 (a) XRD pattern, (b) SEM, (c) TEM, (d) HRTEM, and (e) STEM images of the Cu_3Ge/Ge@G aerogel. Inset in (b) is a digital photograph of the Cu_3Ge/Ge@G aerogel. Insets in (d) are the corresponding Fast Fourier Transform (FFT) patterns of the selected regions marked with the red and white boxes. (f–h) EDS elemental mapping images of the Cu_3Ge/Ge@G aerogel.

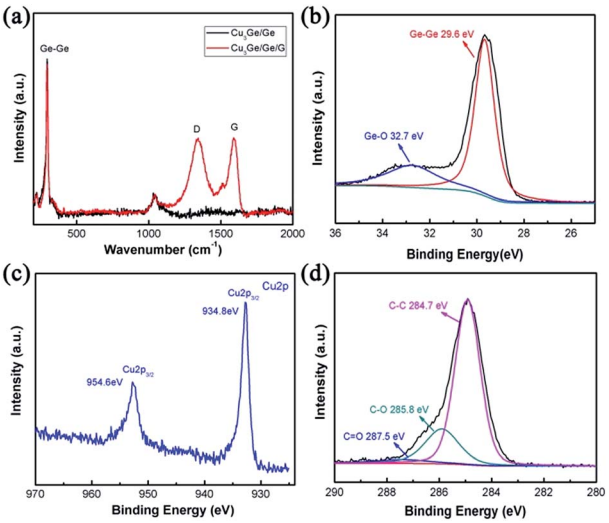

Fig. 3 (a) Raman spectra of the Cu_3Ge/Ge@G aerogel and Cu_3Ge/G. (b), (c) and (d) are the high resolution XPS spectra of Ge 3d, Cu 2p and C 1s in the Cu_3Ge/Ge@G aerogel.

nanoparticle configuration indicates that the improvement of rate capability could be realized by the conductive Cu_3Ge nanoparticles and graphene nanosheets.[7,15] Furthermore, the HRTEM and corresponding FFT images of a Cu_3Ge/Ge nanoparticle in Fig. 2d revealed that the metallic Ge phase is adjacent to the highly conductive Cu_3Ge which implies a fast electron transfer ability in the electrodes. The scanning transmission electron microscopy (STEM) image (Fig. 2e) and energy-dispersive X-ray spectrum (EDS) mappings (Fig. 2f–h) of the Cu_3Ge/Ge@G aerogel confirmed that the Cu_3Ge/Ge nanoparticles are homogeneously embedded in the graphene nanosheet network. Moreover, it should be noted that the distribution of carbon throughout the selected area is quite uniform, suggesting that most of the Cu_3Ge/Ge nanoparticles were homogeneously encapsulated in the conductive graphene nanosheet matrix for a superior lithium storage performance.[2]

Further structural information was acquired by Raman and XPS measurements and displayed in Fig. 3. As shown in the Raman spectra in Fig. 3a, both of the two samples exhibited a sharp peak at 301.5 cm^{-1}, which was attributed to the optical mode of crystalline Ge.[2] Compared with the bare Cu_3Ge/Ge material, the two peaks which appeared at 1336.3 eV and 1589.7 eV in the Cu_3Ge/Ge@G aerogel could be indexed to the D and G bands of the graphene nanosheets, respectively.[14,16] It is worth noting that the unknown peaks at 1039 cm^{-1} in both curves need further assignment. In addition, the surface composition was investigated by XPS analysis. The spectra in Fig. 3b displayed a strong Ge 3d peak at 32.5 eV and a weak shoulder around 30 eV which could be attributed to the slight surface oxidation.[36] For the Cu 2p spectrum (Fig. 3c), the two peaks at 934.8 eV (Cu $2p_{2/3}$) and 954.6 eV (Cu $2p_{1/3}$) were observed due to multiplet splitting. As displayed in the C 1s spectrum of Fig. 3d, a dominant peak centered at 284.9 eV was well assigned to the sp^2 carbon of the graphene nanosheets.[24] Both the Raman and XPS measurements confirmed that the Cu_3Ge/Ge nanoparticles were well incorporated with the graphene nanosheets. In addition, the amount of graphene in the nanocomposite is about 60% according to the TG results as shown in Fig. S3.†

Typical voltage profiles of the Cu_3Ge/Ge@G aerogel at 0.1C (1C = 1384 mA g^{-1} according to $Li_{15}Ge_4$) are presented in Fig. 4a. A flat plateau around 0.3 V was observed in the first discharge curve which was attributed to the formation of a Li–Ge alloy.[29,37] CV curves of the aerogel anode in Fig. S4† displayed lithiated peaks at 0.32 V and delithiated peaks at 0.46 V which correspond to the alloy and dealloy reactions of the Ge nanoparticles, respectively.[38] At the same time, no signals which account for the reactions between the lithium and the Cu_3Ge were detected which means that the Cu_3Ge component was electrochemically inert. This result could be confirmed from the existence of a Cu_3Ge phase in the *ex situ* XRD pattern of the electrode at 5 mV in Fig. S5.†[32] For the first cycles, the discharge and charge capacity are 1655 mA h g^{-1} and 1179 mA h g^{-1}, corresponding to an initial coulombic efficiency of 71%. However, it is only 62% for bare $CuGeO_3$ NWs as reported in Kim's research.[26] For the $CuGeO_3$ and graphene composite anode, the value was even lower (56% and 45.5% as reported by Lin[25] and Song's[24] group). The improved initial coulombic efficiency benefits from the complete removal of oxygen and the electrochemically inert components (binder and conductive

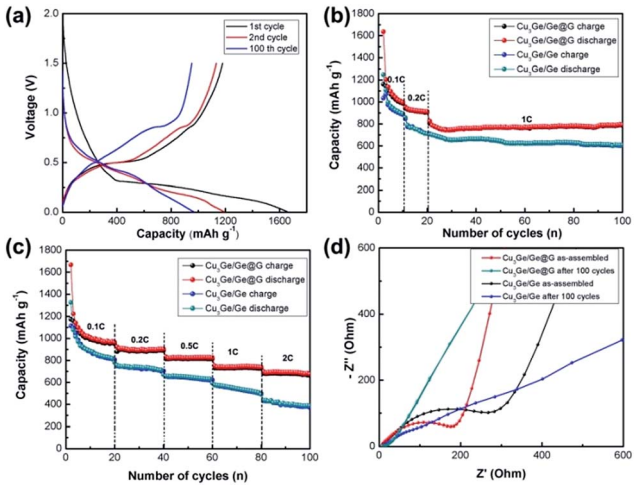

Fig. 4 Electrochemical performances of the Cu_3Ge/Ge@G aerogel and Cu_3Ge/Ge anode. (a) Voltage profile of the Cu_3Ge/Ge@G aerogel at a current density of 0.1C (1C = 1384 mA g^{-1} according to $Li_{15}Ge_4$). (b), (c) and (d) are the cycling performances, rate capabilities and electrochemical impedance spectra, respectively, of the Cu_3Ge/Ge@G aerogel and Cu_3Ge/Ge electrodes.

carbon additive) which results in an irreversible capacity.[3] After 100 charge/discharge cycles at 0.1C, the Cu_3Ge/Ge@G aerogel anode maintained a reversible capacity of 966 mA g^{-1}. Nevertheless, the bare $CuGeO_3$ NWs only offer a capacity of 501 mA g^{-1} after 100 cycles at the same current density as displayed in Fig. S6.† This favorable reliability was related to the graphene enwrapped Ge nanoparticle structure which confined the volume expansion of the Li–Ge alloy. Meanwhile, the cycling stability of the multiphase anodes at a high rate was also measured and displayed in Fig. 4b. At a current density of 1C, the reversible capacities of the Cu_3Ge/Ge@G aerogel anode and the Cu_3Ge/Ge anode were 790 mA h g^{-1} and 608 mA h g^{-1}, respectively. The superior lithium storage capacity of the Cu_3Ge/Ge@G aerogel could be attributed to the introduction of the graphene nanosheets. More importantly, due to the conductive network constructed by the Cu_3Ge nanoparticles and the graphene nanosheets, the rate capability of the aerogel anode was enhanced significantly. As depicted in Fig. 4c, even when cycled at a high current density of 2C, the Cu_3Ge/Ge@G aerogel anode still maintained a reversible capacity of 684 mA h g^{-1}. For comparison, it was only 389 mA h g^{-1} for the Cu_3Ge/Ge electrode. This result implies that the electrons generated during the electrochemical reactions could migrate rapidly in the aerogel anode with a three-dimensional configuration. With the aim to further elucidate the electron diffusion behavior in the two electrodes, electrochemical impedance spectra (EIS) before and after cycling at 1C were obtained. As displayed in Fig. 4d, all the Nyquist plots of the two electrodes were composed of a semicircle and a straight line. Specifically, the semicircle at high frequency represents charge-transfer resistance (R_{ct}), whereas the straight line at low frequency is associated with diffusion resistance through the bulk material. From the Nyquist plots in Fig. 4d and corresponding fitted parameters in Table S1,† it is obvious that the charge-transfer resistance of the Cu_3Ge/Ge@G aerogel (97.8 Ω) is lower than that of the Cu_3Ge/Ge electrode (140.2 Ω) before cycling, which was attributed to the highly conductive graphene nanosheets. Moreover, after 100 cycles at 1C, the semicircle for the Cu_3Ge/Ge@G aerogel was more compressed which implies a more favorable SEI formation for lithium diffusion.[39] Yet, for the sample without graphene, the plot presented an obscure semicircle which indicated a large resistance. This may be caused by the pulverization of the materials and electrical contact failure as the continuous volume of the electrode varies. Furthermore, we checked the morphology of the Cu_3Ge/Ge@G aerogel after 100 discharge/charge cycles, and the results are displayed in Fig. S7.† The microscope images indicate that the Cu_3Ge/Ge nanoparticles are still well-anchored on the surface of graphene nanosheets which accounts for the favorable cycling stability.

Conclusions

In summary, a multiphase Ge aerogel was synthesized *via* a simple pyrolysis of a hybrid mixture of $CuGeO_3$ nanowires and graphene oxide nanosheets. Due to the absence of oxygen and electrochemically inert additives, the irreversible capacity of the Cu_3Ge/Ge@G aerogel was decreased and an enhanced initial columbic efficiency was achieved. A more stable cycling performance was also recorded for the reason of a buffering effect supplied by the two-dimensional graphene. More importantly, the as-formed Cu_3Ge nanoparticle and graphene nanosheet conductive network accelerates the electron diffusion rate in the electrode which results in the superior lithium storage kinetics of the Cu_3Ge/Ge@G aerogel anode. These unique structural features and the favorable electrochemical performance mean the Cu_3Ge/Ge@G aerogel is a promising anode material for lithium batteries.

Acknowledgements

The authors thank the financial support of Qingdao Key Lab of Solar Energy Utilization and Energy Storage Technology, China Postdoctoral Science Foundation (2014M561976), Shandong Provincial Natural Science Foundation (BS2015CL014), National Program on Key Basic Research Project of China (973 Program) (No. MOST2011CB935700), the NSFC program (21271180) and the Key Technology Research Projects of Qingdao (No. 13-4-1-10-gx).

References

1 X. Lu, J. T. Harris, J. E. Villarreal, A. M. Chockla and B. A. Korgel, *Chem. Mater.*, 2013, **25**, 2172–2177.
2 Y. Xu, X. Zhu, X. Zhou, X. Liu, Y. Liu, Z. Dai and J. Bao, *J. Phys. Chem. C*, 2014, **118**, 28502–28508.
3 C. Zhang, Z. Lin, Z. Yang, D. Xiao, P. Hu, H. Xu, Y. Duan, S. Pang, L. Gu and G. Cui, *Chem. Mater.*, 2015, **27**, 2189–2194.
4 G. L. Cui, L. Gu, L. J. Zhi, N. Kaskhedikar, P. A. van Aken, K. Müllen and J. Maier, *Adv. Mater.*, 2008, **20**, 3079–3083.
5 K. C. Klavetter, S. M. Wood, Y.-M. Lin, J. L. Snider, N. C. Davy, A. M. Chockla, D. K. Romanovicz, B. A. Korgel, J.-W. Lee,

A. Heller and C. B. Mullins, *J. Power Sources*, 2013, **238**, 123–136.
6 T. D. Bogart, A. M. Chockla and B. A. Korgel, *Curr. Opin. Chem. Eng.*, 2013, **2**, 286–293.
7 F.-W. Yuan and H.-Y. Tuan, *Chem. Mater.*, 2014, **26**, 2172–2179.
8 H. Jia, R. Kloepsch, X. He, J. P. Badillo, P. Gao, O. Fromm, T. Placke and M. Winter, *Chem. Mater.*, 2014, **26**, 5683–5688.
9 J. Liang, X.-Y. Yu, H. Zhou, H. B. Wu, S. Ding and X. W. Lou, *Angew. Chem., Int. Ed.*, 2014, **53**, 12803–12807.
10 T. Kennedy, E. Mullane, H. Geaney, M. Osiak, C. O'Dwyer and K. M. Ryan, *Nano Lett.*, 2014, **14**, 716–723.
11 M. H. Seo, M. Park, K. T. Lee, K. Kim, J. Kim and J. Cho, *Energy Environ. Sci.*, 2011, **4**, 425–428.
12 X. Lu and B. A. Korgel, *Chem.–Eur. J.*, 2014, **20**, 5874–5879.
13 T. D. Bogart, D. Oka, X. Lu, M. Gu, C. Wang and B. A. Korgel, *ACS Nano*, 2014, **8**, 915–922.
14 J. G. Ren, Q. H. Wu, H. Tang, G. Hong, W. J. Zhang and S. T. Lee, *J. Mater. Chem. A*, 2013, **1**, 1821–1826.
15 J.-G. Ren, Q.-H. Wu, H. Tang, G. Hong, W. Zhang and S.-T. Lee, *J. Mater. Chem. A*, 2013, **1**, 1821–1826.
16 J. Cheng and J. Du, *CrystEngComm*, 2012, **14**, 397–400.
17 W. Tang, Y. Liu, C. Peng, M. Y. Hu, X. Deng, M. Lin, J. Z. Hu and K. P. Loh, *J. Am. Chem. Soc.*, 2015, **137**, 2600–2607.
18 C. Zhang, S. Pang, Q. Kong, Z. Liu, H. Hu, W. Jiang, P. Han, D. Wang and G. Cui, *RSC Adv.*, 2013, **3**, 1336–1340.
19 J. Feng, M. O. Lai and L. Lu, *Mater. Res. Bull.*, 2012, **47**, 1693–1696.
20 F. Zou, X. Hu, L. Qie, Y. Jiang, X. Xiong, Y. Qiao and Y. Huang, *Nanoscale*, 2014, **6**, 924–930.
21 J. Feng, L. Ci, Y. Qi, N. Lun, S. Xiong and Y. Qian, *Mater. Res. Bull.*, 2014, **57**, 238–242.
22 S. Jin and C. Wang, *Nano Energy*, 2014, **7**, 63–71.
23 W. Li, X. Wang, B. Liu, J. Xu, B. Liang, T. Luo, S. Luo, D. Chen and G. Shen, *Nanoscale*, 2013, **5**, 10291–10299.
24 Z. Chen, Y. Yan, S. Xin, W. Li, J. Qu, Y.-G. Guo and W.-G. Song, *J. Mater. Chem. A*, 2013, **1**, 11404–11409.
25 S. Wu, R. Wang, Z. Wang and Z. Lin, *Nanoscale*, 2014, **6**, 8350–8358.
26 G.-H. Lee, J.-C. Kim, D.-H. Lee, S.-D. Seo, H.-W. Shim and D.-W. Kim, *ChemElectroChem*, 2014, **1**, 673–678.
27 R. Chen, T. Zhao, W. Wu, F. Wu, L. Li, J. Qian, R. Xu, H. Wu, H. M. Albishri, A. S. Al-Bogami, D. A. El-Hady, J. Lu and K. Amine, *Nano Lett.*, 2014, **14**, 5899–5904.
28 M. A. Worsley, S. J. Shin, M. D. Merrill, J. Lenhardt, A. J. Nelson, L. Y. Woo, A. E. Gash, T. F. Baumann and C. A. Orme, *ACS Nano*, 2015, **9**, 4698–4705.
29 J. Liu, K. Song, C. Zhu, C.-C. Chen, P. A. van Aken, J. Maier and Y. Yu, *ACS Nano*, 2014, **8**, 7051–7059.
30 H. Wang, C. Zhang, Z. Liu, L. Wang, P. Han, H. Xu, K. Zhang, S. Dong, J. Yao and G. Cui, *J. Mater. Chem.*, 2011, **21**, 5430–5434.
31 R.-Q. Song, A.-W. Xu and S.-H. Yu, *J. Am. Chem. Soc.*, 2007, **129**, 4152–4153.
32 O. B. Chae, S. Park, J. H. Ku, J. H. Ryu and S. M. Oh, *Electrochim. Acta*, 2010, **55**, 2894–2900.
33 G. Gao, H. B. Wu and X. W. Lou, *Adv. Energy Mater.*, 2014, **4**, 1400422.
34 X. Zhou, J. Bao, Z. Dai and Y.-G. Guo, *J. Phys. Chem. C*, 2013, **117**, 25367–25373.
35 Y. Du, X. Zhu, X. Zhou, L. Hu, Z. Dai and J. Bao, *J. Mater. Chem. A*, 2015, **3**, 6787–6791.
36 A. M. Chockla, K. C. Klavetter, C. B. Mullins and B. A. Korgel, *ACS Appl. Mater. Interfaces*, 2012, **4**, 4658–4664.
37 X. Li, Z. Yang, Y. Fu, L. Qiao, D. Li, H. Yue and D. He, *ACS Nano*, 2015, **9**, 1858–1867.
38 Y. Sun, S. Jin, G. Yang, J. Wang and C. Wang, *ACS Nano*, 2015, **9**, 3479–3490.
39 X. Sun, W. Si, L. Xi, B. Liu, X. Liu, C. Yan and O. G. Schmidt, *ChemElectroChem*, 2015, **2**, 737–742.

